www.czasopisma.pan.pl PAN www.journals.pan.pl
Opto-Electronics Review 25 (2017) 80–88

Contents lists available at ScienceDirect

Opto-Electronics Review

journal homepage: http://www.journals.elsevier.com/opto-electronics review

MODELLING of a two-dimensional photonic crystal with line defect for a laser gas sensor application

A. Zakrzewski *, S. Patela

Wroclaw University of Technology, Faculty of Microsystem Electronics and Photonics, 27 Wybrzeże Wyspiańskiego St, Wrocław 50-370, Poland

ARTICLE INFO

Article history:
Received 23 March 2017
Accepted 15 May 2017
Available online 18 May 2017

Keywords:
Photonic crystal
Line defect
Numerical analysis
Laser gas sensor

ABSTRACT

We present the results of a numerical analysis of a two-dimensional photonic crystal with line defect for a laser gas sensor working in a slow light regime. The geometrical parameters of photonic crystals with three different line defects were numerically analyzed: a missing row of holes, a row of holes with changed diameter and air channel. Antireflection sections were also analyzed. The simulations were carried out by MEEP and MPB programs, with the aim to get the values of a group refractive index, transmission and a light-gas overlap as high as possible. The effective refractive index method was used to reduce the simulation time and required computing power. We also described numerical simulation details such as required conditions to work in the slow light regime and the analyzed parameters values' dependency of the simulation resolution that may influence the accuracy of the results.

1. Introduction

Photonic crystals (PhCs) are artificial materials, optical properties of which can be engineered to a wide extent. Of interest for the optical sensor is the possibility of forming absorption spectra and dispersion properties [1–3] according to application requirements. In particular, through manipulation of dispersion the group refractive index, the velocity of light can be slowed down, leading to the so-called "slow light" phenomenon [4,5]. Operation of the gas sensor may be based on absorption spectroscopy where the concentration of the gas is measured through the analysis energy of light absorbed by gas molecules. The use of a slow light phenomenon can enhance the interaction between light and gas medium [6]. However, the increase of the group refractive index (n_g) of the crystal is accompanied by changes in the optical field distribution. This, in turn, results in changes of the light-gas overlap (η) and the transmission coefficients (T). The light-gas overlap coefficient is defined as an energy ratio of the electromagnetic field which propagates in air holes of a photonic crystal to the total energy. The coefficient is of 100% if we assume that light is guided outside the material forming a photonic crystal. In this case, theoretically, interaction efficiency is increased by a factor equal to the value of a group refractive index. The third important parameter, for optical gas sensors, is a transmission coefficient which should be maximized to maintain a good signal-to-noise ratio at the receiver. The unique feature of gas sensors based on photonic crystals is the possibility to obtain high values of all three (n_g, η, T) coefficients by a proper design of the photonic crystal structure.

In this paper we present results of an analysis and optimization of the photonic crystal structure, aiming at maximizing the η, n_g and T coefficients, to make the crystal usable in optical gas sensors. An additional calculation complication arises from the fact, that the crystal has to be tuned to a required wavelength of light and an optical band structure has to be taken into account. The band structure should take into account defect modes useful for the optical sensor design. Considering all mentioned requirements and parameters, we define a working point of the device. We choose the working point in the range of a defect mode localized within the photonic band gap. The defect mode occurs because of a disorder introduced into the periodic structure of the photonic crystal. We analyzed a PhC with three types of line defects. For the photonic crystal, we selected a triangular lattice of holes because it provides a greater tolerance of work in the range of a chosen mode. The analysis carried out in this article was performed to optimize the gas sensor, but the method of the analysis can be used while constructing other devices based on photonic crystals.

2. The concept of the laser gas sensor

A short description of the concept of the sensor is provided below. Technological details of our laser gas sensor based on a two-dimensional photonic crystal have been presented elsewhere

* Corresponding author.
E-mail address: adrian.zakrzewski@pwr.edu.pl (A. Zakrzewski).

http://dx.doi.org/10.1016/j.opelre.2017.05.002
1896-3757/

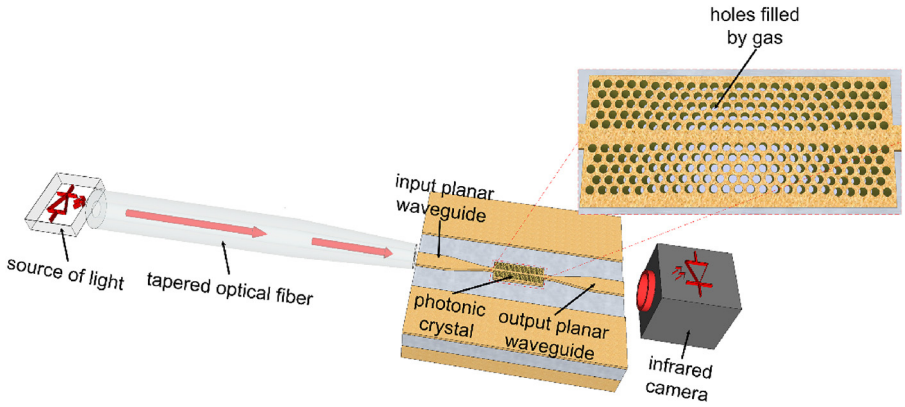

Fig. 1. The design of gas sensor based on a two-dimensional photonic crystal fabricated in a silicon-on-insulator heterostructure.

[7]. Our sensor, based on a two-dimensional photonic crystal, was fabricated in a silicon-on-insulator heterostructure (SOI) by an e-beam lithography (EBL) and a reactive ion etching (RIE). The gas sensor consisted of a tuneable semiconductor laser, a tapered optical fiber, a 2D photonic crystal working in the slow light regime, and an infrared camera (Fig. 1). The principle of operation of the gas sensor is based on measurements of a single-wavelength light transmission through a photonic crystal which holes are filled with gas. The wavelength of the source of light should correspond to the wavelength of the absorption peak of gas undergoing the detection. The wavelength selected for this work was suitable for a detection of acetylene for which a strong absorption peak occurs at $\lambda_0 = 1531.588$ nm [8].

The active element of the sensor included a photonic crystal waveguide with input and output strip waveguides and tapered sections between them (Fig. 2). Waveguides consisted of three parts: initial, the widest one ($W_1 = 15$ μm and length $L_1 = 10$ μm), intermediate, the longest $L_2 = 800$ μm and the final section characterized by width W_3 close to 1 μm and length $L_3 = 10$ μm. The tapered optical fibre was used to improve the efficiency of light coupling into an active element of the sensor. Parameters of all the mentioned sections were analyzed and optimized by us for the best sensor operation [7].

The numerical analysis was carried out for photonic crystals with three sorts of line defects including one row of missing holes, one row of holes with changed diameters and an air channel (Fig. 3).

We carried out the numerical analysis with the MEEP (MIT Electromagnetic Equation Propagation) [9] and MPB (MIT Photonic-Bands) [10] packages. The MEEP software, based on a finite-difference time-domain (FDTD) method, was used for transmission and group refractive index characterization of PhC. The MPB software based on definite-frequency eigenstates of Maxwell's equations was used to get photonic band diagrams (PBD) of PhC and to calculate a light-gas overlap.

3. Effective refractive index method

In general, the numerical analysis should be performed in three dimensions, where length, width, and thickness of a structure are defined. However, such approach is time-consuming and requires substantial numerical power. The computational requirements are lowered if a 3D model is replaced with a 2D one. For a planar waveguiding structure, a photonic crystal waveguide exhibits refractive index periodicity in two dimensions so that it can be modeled with a good approximation as a two-dimensional structure. The three-dimensional model can be approximated by two-dimensional one, under the condition that refractive index of the guiding material is replaced with an effective refractive index of a planar waveguide [11,12]. The approach is called Effective Refractive Index method and was used in our analysis. In that method, the photonic crystal fabricated and analyzed numerically is characterized by the effective refractive index which represents both thickness and refractive index of the structure.

The effective refractive indices of the waveguiding modes may be calculated using the mode Eq. (1) of planar waveguides [11]. The equation is solved by finding zeros of the function:

$$\left(\frac{2\pi h}{\lambda}\right)\sqrt{(n_w^2 - N_{eff}^2)} = m\pi + tan^{-1}\left[C_1\sqrt{\frac{N_{eff}^2 - n_c^2}{n_w^2 - N_{eff}^2}}\right] + tan^{-1}\left[C_2\sqrt{\frac{N_{eff}^2 - n_s^2}{n_w^2 - N_{eff}^2}}\right] \quad (1)$$

where N_{eff} is the effective refractive index of the guiding layer, n_w, n_s, n_c are the refractive indices of guiding, top and bottom layer, respectively, λ is the wavelength, h is the guiding layer thickness, m is the mode number, $C_1 = C_2 = 1$ for TE polarization, $C_1 = {n_w}^2/{n_c}^2$ and $C_2 = {n_w}^2/{n_s}^2$ for TM polarization.

The effective refractive index of a guiding layer in which PhC was fabricated was calculated for the wavelength $\lambda_0 = 1531.588$ nm and the refractive indices $n_{Si} = 3.48$ [13], $n_{SiO2} = 1.44$ [14] (Fig. 4).

Single mode propagation of light through a photonic crystal was obtained for the thickness of a guiding layer equal to or less than 275 nm. The thickness 220 nm was chosen for further analysis. The effective refractive index N_{eff} was close to 2.74 for the TE polarization for which the gas sensor was designed. The TE polarization was selected because of the availability of the defect mode inside the photonic bandgap (for the triangular lattice 2D PhC) [15].

4. Numerical analysis of photonic crystals

The triangular-lattice photonic crystals with three different line defects were analyzed numerically to obtain as high as possible values of transmission, group refractive index, and light-gas overlap. The task definition is straightforward. However, the analysis itself is intricate, extensive and poses several risks. Details on calculating light-gas overlap coefficient, establishing numerical resolution and selecting a working point of the sensor within the slow light regime are described in this paper. Further, a general methodology of modelling photonic-crystal-based devices is provided.

4.1. Light-gas overlap coefficient

Modelling software, in general, is composed of three parts: input functions, proper calculation engine, and output functions. The output functions of the MPB software provide values of material

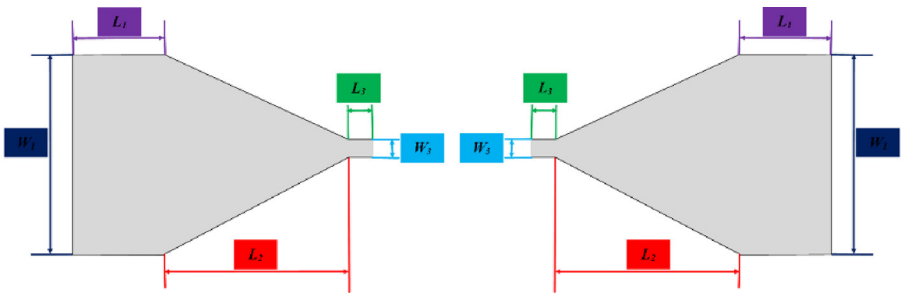

Fig. 2. The configuration of photonic crystal input and output strip waveguides and tapered sections between them.

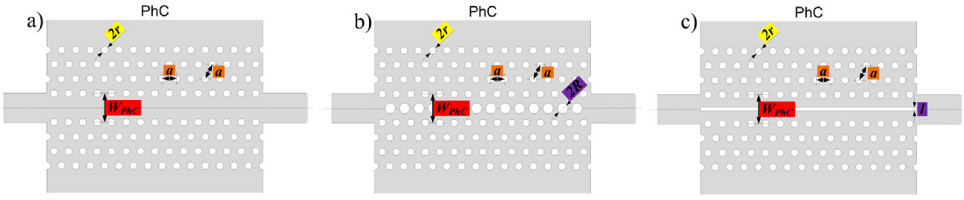

Fig. 3. Illustration of structures and parameters discussed in the paper; three sorts of line defects are shown: (a) one row of missing holes, (b) row of holes changed diameter, and (c) air channel.

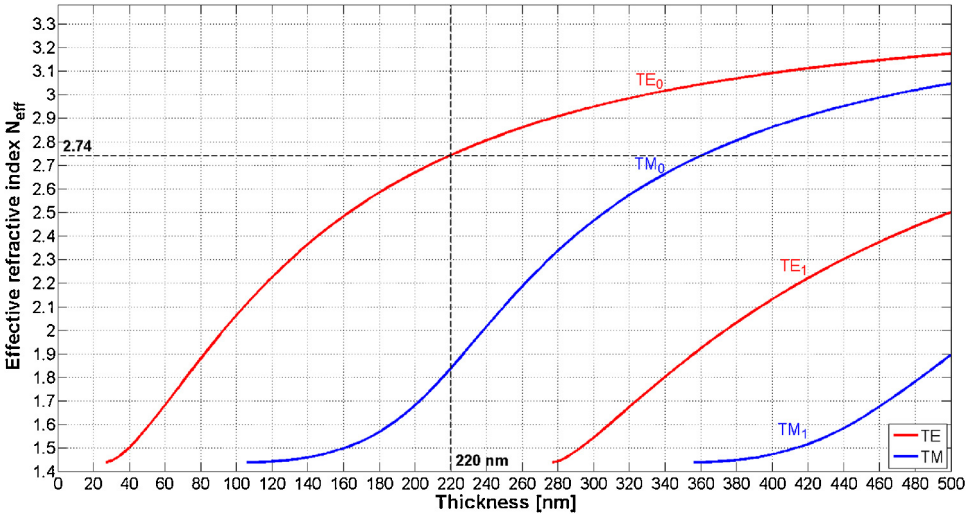

Fig. 4. Effective refractive index dependence on the thickness of guiding layer in which PhC was fabricated.

parameters (such as effective refractive indices) and information about distribution of electromagnetic field (such as intensity). The values of the effective refractive index and the intensity of electromagnetic field in each computing cell are stored in an hdf format, designed to store and organize large amounts of data. The data are organized in two groups of objects. The slave type is composed of a dataset containing multidimensional arrays. The master type holds datasets. The number of computing cells depends on the size of the analyzed structure and the resolution of simulation. Generated data stored in an hdf format can be later processed by an external program, in our case by Matlab software. Each computing cell can represent the free space around the structure, air holes or the bulk material of the guiding layer. The integrals of electromagnetic field intensity over volumes of air holes and guiding layer were determined. The ratio of these integrals is called a light-gas overlap coefficient. The high value of this coefficient is essential for high sensitivity of gas sensors and is a good illustration of the interaction area within a sensor, as illustrated in Fig. 5. Fig. 5a represents the geometry of the structure, with e epsilon of the guiding layer close to 7.51. Fig. 5b shows the distribution of the electromagnetic field in the whole structure, while Fig. 5c illustrates how the field looks like in the holes, where the interaction of light with gas takes place.

4.2. Simulation resolution

We set the dimension of a single cell in the calculation grid to 2 nm what corresponded to the program simulation resolution of 200. This value of the resolution ensured convergence of the numerical procedure. As an example, the overlap coefficient η *vs.* simulation resolution is shown in Fig. 6, the result is converging exponentially toward the final value. Additionally, to improve the efficiency of calculations, the symmetry of the analyzed structure is taken into account; this is done numerically by the introduction of a symmetry plane along the structure. Finally, "perfect matched layers" (PML) were implemented. The PMLs eliminate unreal "reflections" of the electromagnetic field from the boundaries of a calculation area. The use of PML layers in an FDTD method was first proposed by Berenger [16]. The PML layers should surround the whole analyzed structure and completely absorb light

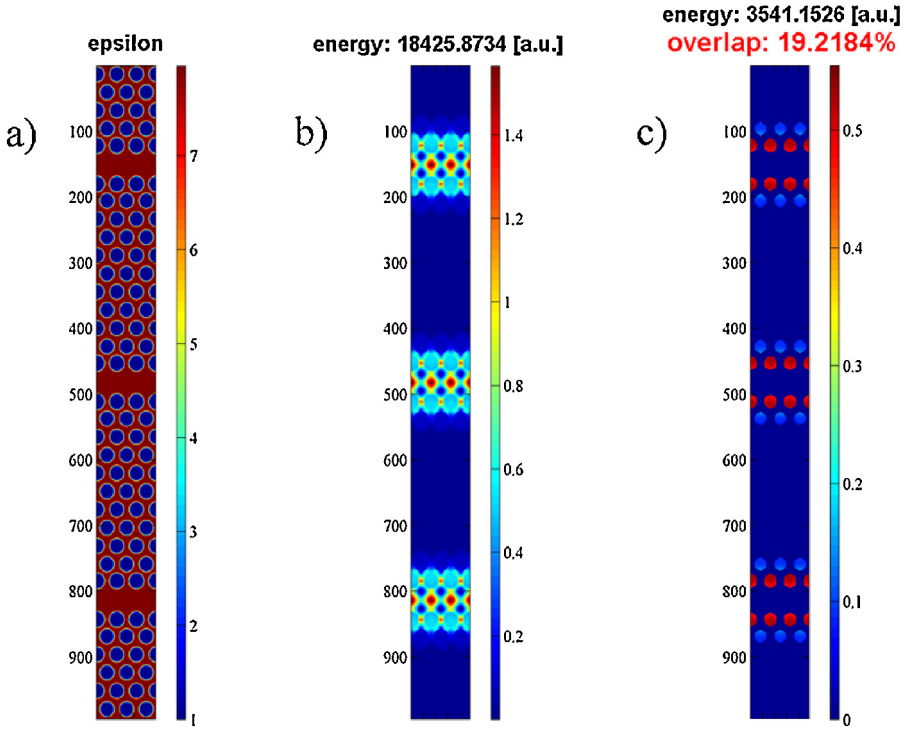

Fig. 5. Electromagnetic field distribution used for calculations of the light-gas overlap coefficient, (a) schematic of analyzed PhC structure, (b) the electromagnetic field intensity in air holes and guiding layer, and (c) the electromagnetic field intensity in air holes only.

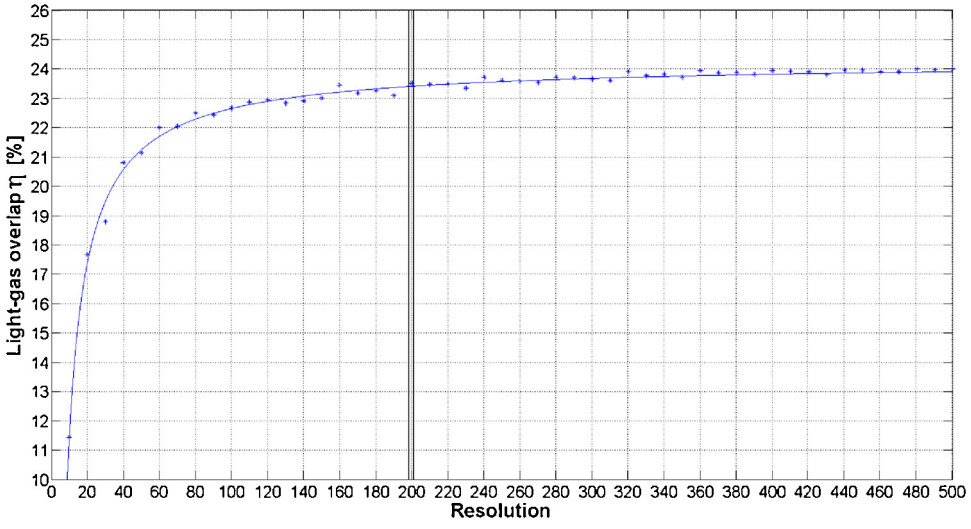

Fig. 6. Light-gas overlap dependency of the simulation resolution.

that reaches them, regardless of the frequency and the direction of incidence.

4.3. The working point

Principle of operation of the gas sensor is based on the slow light phenomenon, through which enhancement of the interaction between the light and gas medium is obtained. Operation in the slow light regime requires that the working point is selected in the spectral range of the strong modal dispersion. Strong dispersion occurs in the vicinity of the bandgap but is usually accompanied by a significant attenuation. Another method of obtaining a strong dispersion is the introduction of a defect into a perfect structure of a photonic crystal and the use of the created defect mode. For using the defect mode, a working point should be established, i.e. a point of normalized frequency for a selected normalized wavevector. The character of PBG and defect mode is dependent on geometrical parameters of the structure. Two different situations are shown in Fig. 7. The first one, when light propagates through a PhC waveguide simply limited by the photonic-bandgap material (gray point, low n_g), and the second when propagation occurs in the slow light regime (purple point, high n_g).

4.4. Lack of work in slow light regime

Optical parameters the optical gas sensor, such as light-gas overlap, transmission, and group refractive index are related to geometrical parameters of the photonic crystal [7]. The parame-

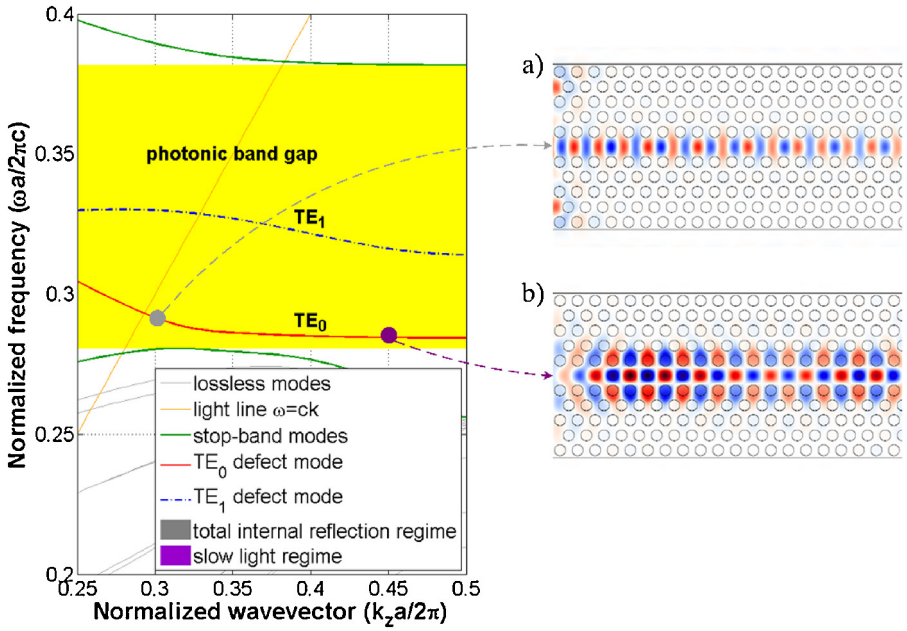

Fig. 7. Photonic band diagram on which two working points were distinguished: (a) gray – propagation established by the PBG-material boundaries, (b) purple – propagation in the slow light regime.

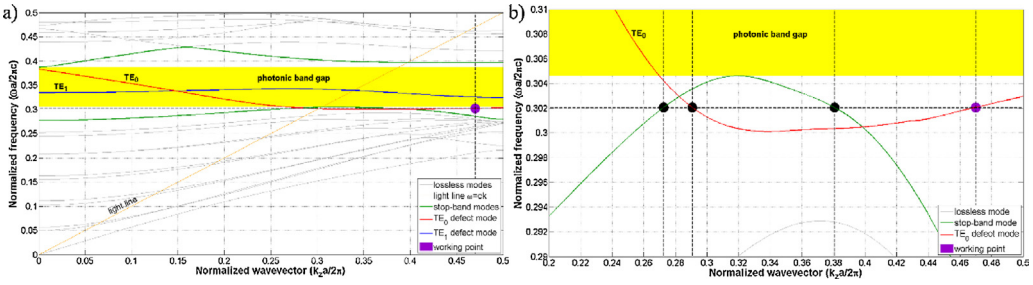

Fig. 8. The example of photonic band diagram showing undesirable phenomenon, i.e. mode degeneracy, and possibility of propagation outside of the slow light regime. (a) A general picture and (b) magnifies the region of interest.

ters should be tuned, to optimize the sensor behaviour. However, the parameters cannot be changed independently. On one hand, the requirements of manufacturing process impose some restrictions, e.g. the holes' radius cannot be too high. On the other hand, if the values of parameters are assigned arbitrarily, problems may arise. For example, the degeneracy of the guided modes may arise, as presented in Fig. 8. The normalized frequency of TE_0 mode corresponding to the wavevector $k = 0.47$ was chosen for numerical analysis (purple circle in Fig. 8). However, if due to the poor design, the mode degeneracy occurs at this point, the eigenfrequency corresponds also to the lower values of a wavevector ($k = 0.27$, $k = 0.29$ and $k = 0.38$) marked by a black circle in Fig. 8b. The dispersion characteristics of TE_0 mode becomes increasingly flat with increasing values of the wavevector k. Therefore, the closer to $k = 0.5$ the higher probability to observe an undesirable phenomenon, like mode mixing or lack of work in the slow light regime. Hence, the $k = 0.47$ was chosen to prevent this situation.

4.5. *The methodology of numerical analysis*

The numerical analysis was carried out for three different line defects created in the triangular-lattice photonic crystals. In this section, we present our methodology of analysis on the example of a line defect including one row of missing holes (Fig. 3a).

The numerical studies were divided into three main steps (Fig. 9). In the first, basic parameters of the structure, such radius of holes r and the width of line defect W_{PhC} were analyzed (Fig. 9a). In the second step of the analysis, parameters of the line defect (radius r_1, r_2 of holes in two rows and the shift p_1, p_2 of two rows of holes) were modeled. In the final step, the parameters related to the antireflection sections AR, such as the holes' radius r_{AR}, the length of these sections L_{AR} and the width of line defect W_{AR} were included into consideration. In all steps, geometrical parameters were analyzed simultaneously.

In the first step, the radius of holes r was varied in the range from $0.1a$ to $0.5a$ with step $0.01a$, and the width of line defect W_{PhC} varied from *W0.80* ($0.8\sqrt{3}a$) to *W1.20* ($1.20\sqrt{3}a$) with step $0.05\sqrt{3}a$. The PBDs were calculated for these values and areas in which an undesirable phenomenon of mode degeneracy does not occur were established (Fig. 10). The normalized frequency of the defect mode for $k = 0.47$ was also calculated. The values of the light-gas overlap coefficient are shown in the figure also.

The photonic crystal built to work in the range marked in Fig. 10 may be used as an active element of gas sensors, as PhC designed in that way allows to define unambiguously a working point for work in the slow-light regime. The indicated contours show that with increasing holes' radius the light-gas overlap increases also. This coefficient decreases with the width of the line defect. Based on this

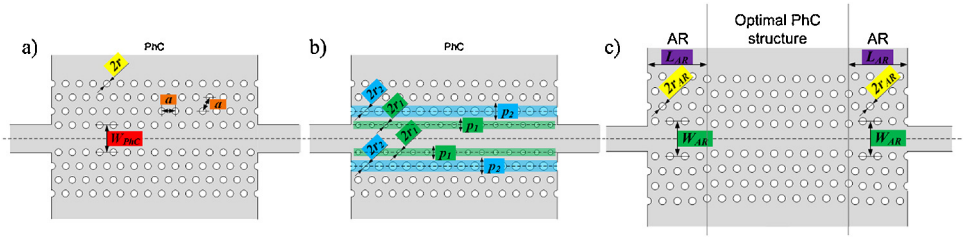

Fig. 9. Illustration of structures and parameters discussed in the paper; three main steps of numerical analysis: (a) basic parameters, (b) parameters of holes and rows near the line defect (c) antireflection sections parameters.

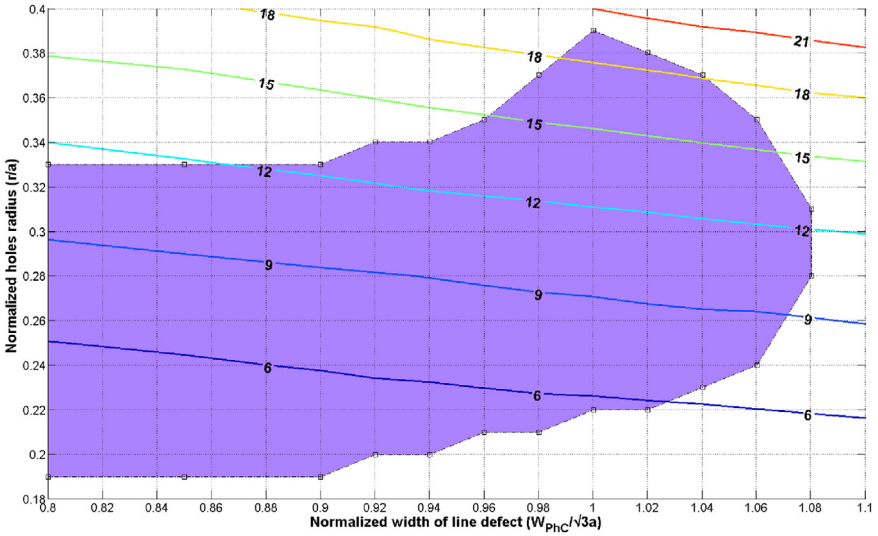

Fig. 10. Normalized holes' radius dependence of the normalized width of a line defect. Purple colour distinguished the working area in which an undesirable phenomenon of mode degeneracy does not occur. The lines represent the value of the light-gas overlap coefficient.

Table 1
The numerical results obtained after the first stage of the optimization process.

Optical parameters	Maximum value	Geometrical parameters	
		r	W_{PhC}
Transmission T [%]	72	$0.28a$	$0.98\sqrt{3}a$
Light-gas overlap η [%]	19.2	$0.39a$	$1.00\sqrt{3}a$
Group refractive index n_g	685	$0.35a$	$0.96\sqrt{3}a$

information it can be deduced that width of the electromagnetic field distribution in a slow light regime is approximately constant along the line defect.

The transmission and group refractive index characteristics (Fig. 11) were determined for geometrical parameters' values included in a working area distinguished in Fig. 10 and for defined normalized frequency.

Parameters of the photonic crystals, obtained after the first stage of optimization process are presented in Table 1.

The maximum values of the optical parameters corresponded to different values of geometrical parameters of the structure. Therefore, to establish parameters of the maximum of the merit function was found, with the weight of each optical parameter set to 1/3. So that, the PhC defined as $W_{phc} = 0.98^{\sqrt{3}}a$ and $r = 0.36a$ and characterized by $T = 58.09\%$, $\eta = 14.73\%$, $n_g = 577.98$ was chosen for further analysis.

The radius of holes in two rows (r_1, r_2) and shift of two rows of holes (p_1, p_2) near line defect were analyzed in the second stage. This part of optimization was divided into two parts: first r_1 and r_2 were changed, later p_1 and p_2. The r_1 and r_2 parameters were changed from $0.1a$ to $0.5a$ with step $0.01a$ and p_1, p_2 parameters from $-0.1a$ to $0.1a$ with step $0.005a$. The obtained results are summed up in Tables 2 and 3.

The values of all three optical parameters from Table 1 increased after an optimization process of r_1 and p_1. The largest increase was achieved in the case of a group refractive index (from 577.98 to 1375.20).

In summary, the group refractive index was increased from 1375.20 to 2031.09 after next stage of the optimization process, while the transmission and light-gas overlap decreased. However, the increase of n_g parameter is much higher than the decrease of T and η parameters.

The antireflection sections were added in the last stage of the numerical optimization to obtain a higher transmission coefficient [17,18]. These AR sections were defined as the region of PhC with different geometrical parameters which included the width of line defect W_{AR}, length L_{AR} and radius of holes r_{AR}. The values were analyzed as follows: W_{AR} was changed from *W0.80* ($0.8^{\sqrt{3}}a$) to *W1.20* ($1.20^{\sqrt{3}}a$) with step $0.05^{\sqrt{3}}a$, L_{AR} from 1 to 15 with step 1 and r_{AR} from $0.1a$ to 0.5a with step $0.01a$. The transmission coefficient increased from 57.18% to 92.45% after the last stage of the optimization process (Fig. 12). This result was obtained for $W_{AR} = 1.06^{\sqrt{3}}a$, $L_{AR} = 5$ and $r_{AR} = 0.22a$.

The final results of the numerical analysis carried out for the photonic crystal with three different line defects are collected in Table 4.

The low value of the group refractive index $n_g = 187.50$ obtained for the air channel line defect, makes the structure uninteresting for laser gas sensors. The PhC with a line defect defined by a row of holes with changed diameter has a higher effective refractive index but a lower transmission coefficient. Therefore, a 2D PhC structure

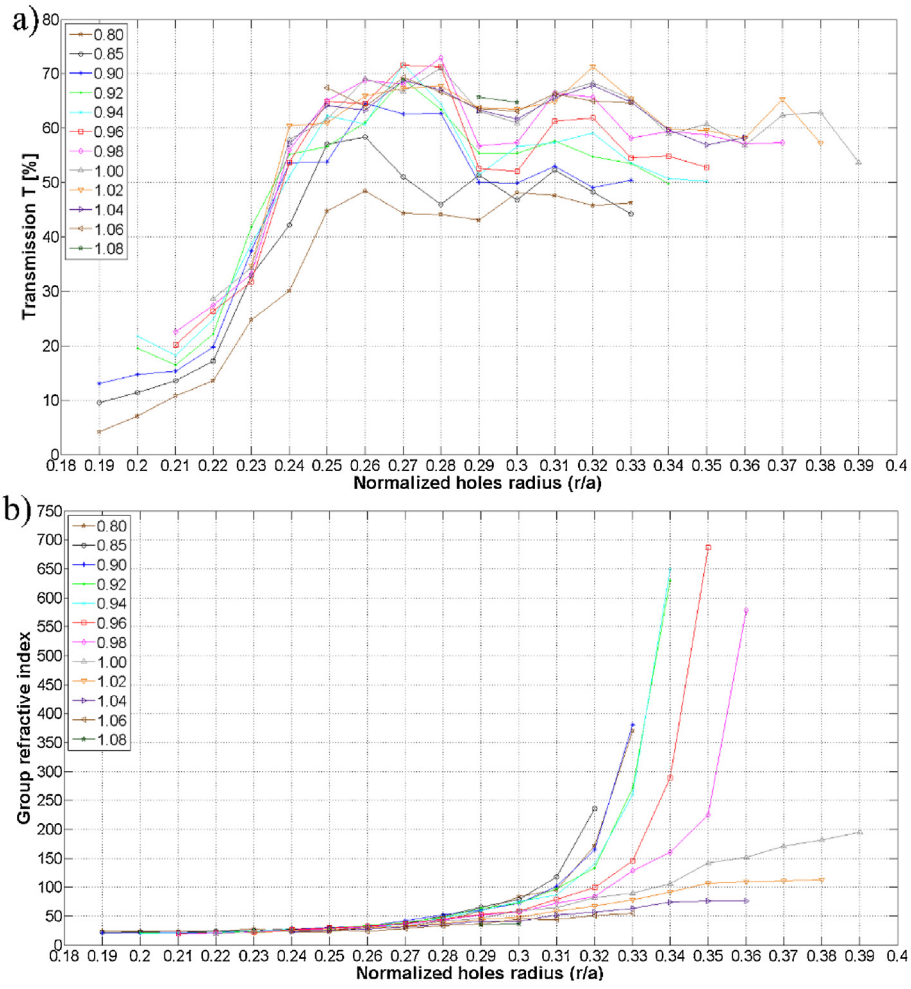

Fig. 11. Transmission (a) and group refractive index (b) dependence of normalized holes' radius for a different width of line defect (details explained in the legend).

Table 2
The numerical results obtained after the first part of the second stage of the optimization process.

	r	W_{PhC}
Starting geometrical parameters defined based previous optimization stage	$0.36a$	$0.98\sqrt{3}a$
Working area	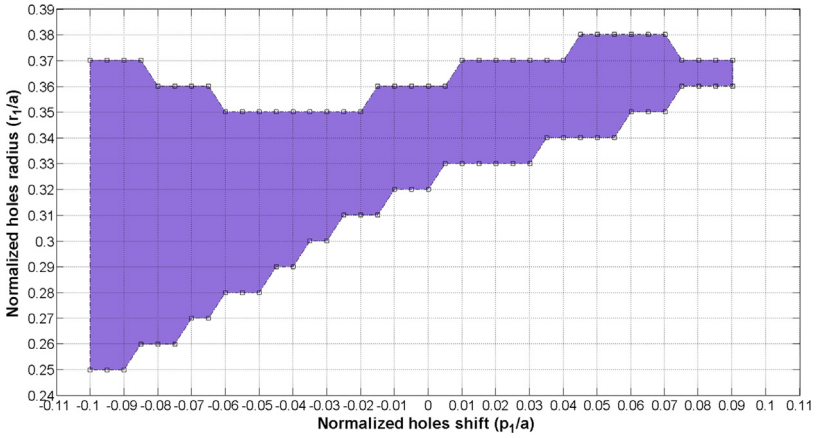	
Best geometrical parameters after first part of second optimization stage	$r_1 = 0.37$a	$p_1 = 0.010$a
Transmission T [%]	**64.32** (58.09)	
Light-gas overlap η [%]	**15.27** (14.73)	
Group refractive index n_g	**1375.20** (577.98)	

The bold values correspond to the maximum values obtained after each stage of the optimization process.

Table 3
The numerical results obtained after the second part of the second stage of the optimization process.

	r	W_{PhC}	r_1	p_1
Starting geometrical parameters defined based on previous optimization stage	$0.36a$	$0.98\sqrt{3}a$	$0.37a$	$0.010a$
Working area	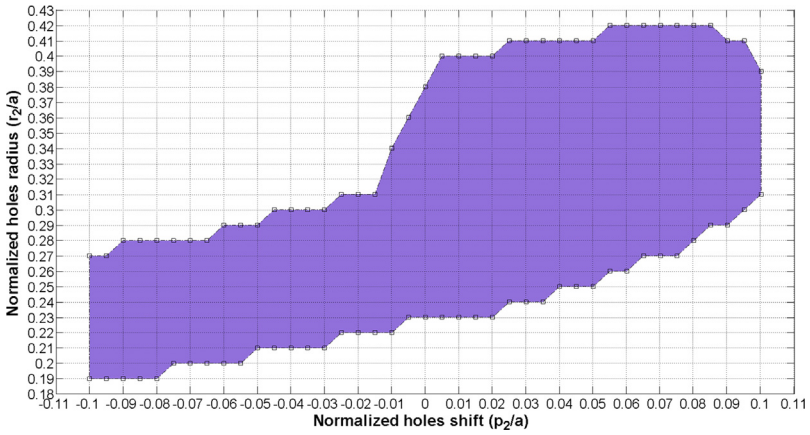			
Best geometrical parameters after second part of second optimization stage	$r_1 = 0.37a$		$p_1 = 0.010a$	
Transmission T [%]	**57.18** (64.32)			
Light-gas overlap η [%]	**14.59** (15.27)			
Group refractive index n_g	**2031.09** (1375.20)			

The bold values correspond to the maximum values obtained after each stage of the optimization process.

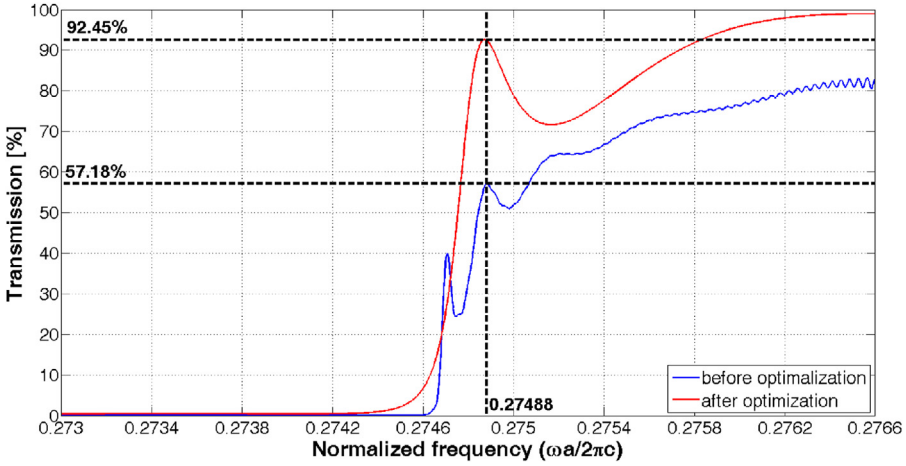

Fig. 12. Transmission coefficient *vs.* normalized frequency; blue and red line – characteristics before and after optimization process of AR sections, respectively.

Table 4
The results of the numerical analysis carried out for the photonic crystal with three different line defects.

		Line defect		
		Missing one row of holes	Row of holes with smaller/larger diameter than others	Air channel
Optical parameters	T [%]	**92.45**	52.64	74.23
	n_g	**2031.09**	1558.71	187.50
	η [%]	**14.59**	15.99	14.62
Geometrical parameters	r	$0.36a$	$0.44a$	$0.43a$
	W_{PhC}	$0.98\sqrt{3}a$	$0.96\sqrt{3}a$	$1.06\sqrt{3}a$
	R	–	$0.21a$	–
	l	–	–	$0.125\sqrt{3}a$

The bold values correspond to the maximum values obtained after each stage of the optimization process.

with missing one row of holes should be an active element of the laser gas sensor.

5. Conclusions

We presented the procedure and results of numerical optimization of a photonic crystal used as an active element of the laser gas sensor [7].

The effective refractive index method was used to reduce the simulation time and computing power required for simulations. Based on the theory of the planar waveguide we obtained the effective refractive index N_{eff} of 2.74 for a 220 nm thick silicon guiding layer, a 1531.588 nm wavelength, and a TE polarization.

The numerical analysis was carried out by MPB and MEEP for three different line defects formed by a missing row of holes, a row of holes with changed diameter and an air channel. The line defect in the photonic crystal structure is necessary to work in the slow light regime with a high transmission of the active waveguide. Working point of the sensor was set in the range of a defect mode localized in the photonic band gap. We did it by selecting the normalized frequency of the mode which corresponds to the value of a wavevector of 0.47. This working point location depends on geometrical parameters of the PhC structure. However, not all values of geometrical parameters can be considered because of the undesirable phenomenon, i.e. the lack of work in the slow light regime. We started our analysis by establishing the working space of a slow-light sensor. Then, within the working space, we analyzed the geometrical parameters of the PhC to obtain the highest possible values of the group refractive index n_g, transmission T, and light-gas overlap η. The light-gas overlap was calculated by the Matlab software as the ratio of electromagnetic fields intensity in air holes to electromagnetic fields intensity in a guiding layer.

The numerical procedure was divided into three steps. In the first step, main parameters (holes radius and width of line defect) were considered. In the second step, tuning of the line defect was performed. This was done by modifying the diameter of some holes and changing the width of the air channel. In the last step, the radius and shift of the first and second row of holes were also taken into consideration to create antireflection sections. The parameters were analyzed simultaneously at all steps. Consequently, a big map of parameters was obtained, and we chose the best structure which is a photonic crystal with the line defect formed by missing one row of holes characterized by the maximum values of interesting parameters ($n_g = 2031.09$, $T = 57.18\%$ and $\eta = 14.59\%$). After the optimization of the antireflection sections, the transmission coefficient increased from 57.18% to 92.45%.

In this paper, we proved that it is possible to design a structure of a two-dimensional photonic crystal which will have simultaneously high values of group refractive index, transmission, and light-gas overlap. The obtained properties may be used for a significant reduction in the required length of the light-gas interaction in a gas sensor working in the slow light regime [7].

Acknowledgements

This paper was supported by Poland National Science Centre, project No. 2011/03/N/ST7/00451 “Analysis of slow light phenomenon in two-dimensional line defect photonic crystal”.

Calculations have been carried out using resources provided by Wroclaw Centre for Networking and Supercomputing (http://wcss.pl).

References

[1] X. Liu, S. Cheng, H. Liu, S. Hu, D. Zhang, H. Ning, A survey on gas sensing technology, Sensors 12 (7) (2012) 9635–9665, http://dx.doi.org/10.3390/s120709635.
[2] B. Troia, A. Paolicelli, F. De Leonardis, V.M.N. Passaro, in: V.M.N. Passaro (Ed.), Photonic Crystals for Optical Sensing: A Review, 2013, http://dx.doi.org/10.5772/53897, ISBN 978-953-51-0954-9.
[3] A. Lambrecht, S. Hartwig, S.L. Schweizer, R.B. Wehrspohn, Miniature infrared gas sensors using photonic crystals, Proc. SPIE 6480, Photonic Crystal Materials and Devices VI (2007), http://dx.doi.org/10.1117/12.700792.
[4] J. Khurgin, R. Tucker, Slow Light Science and Applications, CRC Press, Florida, 2009.
[5] A. Figotin, I. Vitebsky, Slow light in photonic crystals, Waves Random Complex Media 16 (3) (2006) 293–382, http://dx.doi.org/10.1080/17455030600836507.
[6] S. Chakravarty, W. Lai, Y. Zou, C. Lin, X. Wang, R.T. Chen, Silicon nanomembrane based photonic crystal nanostructures for chip-integrated open sensor systems, Proc. SPIE **8198**, International Conference on Optical Instruments and Technology: Optoelectronic Devices and Integration (2011), http://dx.doi.org/10.1117/12.910878.
[7] A. Zakrzewski, and S. Patela, “Investigation of the laser acetylene sensor based on two-dimensional photonic crystal”, (in preparation).
[8] HITRAN2008. https://www.cfa.harvard.edu/hitran/.
[9] A.F. Oskooi, D. Roundy, M. Ibanescu, P. Bermel, J.D. Joannopoulos, S.G. Johnson, MEEP: a flexible free-software package for electromagnetic simulations by the FDTD method”, Comput. Phys. Commun. 181 (3) (2010) 687–702, http://dx.doi.org/10.1016/j.cpc.2009.11.008.
[10] J. Joannopoulos, S.G. Johnson, Block-iterative frequency-domain methods for Maxwell’s equations in a planewave basis”, Opt. Express 8 (3) (2001) 173–190, http://dx.doi.org/10.1364/OE.8.000173.
[11] C.G. Bostan, R.M. de Ridder, V.J. Gadgil, H. Kelderman, L. Kuipers, A. Driessen, Design and fabrication of line-defect waveguides in hexagon-type SOI photonic crystal slabs, Proc. SPIE **5450**, Photonic Crystal Materials and Nanostructures (2004), http://dx.doi.org/10.1117/12.545694.
[12] H.Y. Ryu, J.K. Hwang, Y.H. Lee, Conditions of single guided mode in two-dimensional triangular photonic crystal slab waveguides”, J. Appl. Phys. 88 (9) (2000) 4941–4946, http://dx.doi.org/10.1063/1.1314300.
[13] H.H. Li, Refractive index of silicon and germanium and its wavelength and temperature derivatives”, J. Phys. Chem. Ref. Data 9 (1980) 561, http://dx.doi.org/10.1063/1.555624.
[14] L. Gao, F. Lemarchand, M. Lequime, Exploitation of multiple incidences spectrometric measurements for thin film reverse engineering, Opt. Express 20 (14) (2012) 15734–15751, http://dx.doi.org/10.1364/OE.20.015734.
[15] S.G. Johnson, P.R. Villeneuve, S. Fan, J.D. Joannopoulos, Linear waveguides in photonic-crystal slabs”, Phys. Rev. B 62 (12) (2000) 8212–8222, http://dx.doi.org/10.1103/PhysRevB.62.8212.
[16] J.P. Berenger, A perfectly matched layer for the absorption of electromagnetic waves, J. Comput. Phys. 114 (2) (1994) 185–200, http://dx.doi.org/10.1006/jcph.1994.1159.
[17] P. Pottier, M. Gnan, R. De La Rue, Efficient coupling into slow-light photonic crystal channel guides using photonic crystal tapers”, Opt. Express 15 (11) (2007) 6569–6575, http://dx.doi.org/10.1364/OE.15.006569.
[18] K. Dossou, L.C. Botten, C.M. de Sterke, R.C. McPhedran, A.A. Asatryan, S. Chen, J. Brnovic, Efficient couplers for photonic crystal waveguides, Opt. Commun. 265 (1) (2006) 207–219, http://dx.doi.org/10.1016/j.optcom.2006.02.052.